Active and Passive Electronic Components
Volume 2008 (2008), Article ID 247958, 6 pages
doi:10.1155/2008/247958

Research Article

Material Parameter Measurements for Microwave Antireflection Coating Development

Lajos Nagy

Department of Broadband Infocommunications and Electromagnetic Theory, Budapest University of Technology and Economics, Goldmann György tér 3, 1111 Budapest, Hungary

Received 3 December 2007; Accepted 17 March 2008

Academic Editor: Tibor Berceli

Abstract

The main steps for characterization and measurement of microwave absorbent materials in the 1–10 GHz range are introduced. The coaxial reflection-transmission type of material parameter measurement is analyzed in detail and the main measurement error is corrected. The microscopic material particle parameter measurement concept is also presented using different mixing rule laws to determine the material parameters of the single particles from the macroscopic parameters. Two-dimensional FDTD simulations have been used to model the behavior of mixed electric and magnetic type of material.

1. Introduction

Antireflection coatings are widely used for optical and high-frequency applications such as microwave absorbing materials for electromagnetic compatibility or decreasing RCS for stealth applications. Even though a single-layer coating may be sufficient to obtain low reflection coefficients, its efficiency is usually reduced to a narrow bandwidth and to a specific polarization and incidence angle.

In order to extend the performance of antireflection coatings to wider ranges of frequency and incidence, a multilayered structure has to be considered.

The optimization of such complex architectures may consist in measurement of macroscopic and microscopic material parameters. This article presents a new calibration flow graph analysis and analytical equation to evaluate the correcting terms. Measurement and simulated results are presented to validate the calibration proposed and to correct the sample size deviation [1].

2. Measurements

2.1. Macroscopic Material Parameter Measurements

The material samples are placed in a coaxial line and two complex parameters are measured, the reflection and the transmission coefficients.

The widely used measurement method of macroscopic material parameters is based on the Nicolson and Ross system. A sample of material which has complex relative permittivity ε_R and permeability μ_R fills a coaxial waveguide section, as shown in Figure 1. TEM electromagnetic wave is propagated along the coaxial line with the material sample and the scattering parameters (S_{11} and S_{12}) are measured using reference planes on the two faces of the sample. The closed form equations derived by Nicolson and Ross are the following:

$$\begin{gathered} V_1 = S_{21} + S_{11}, \\ V_2 = S_{21} - S_{11}, \\ \Gamma = \frac{1 - V_1 V_2}{V_1 - V_2} \pm \sqrt{\left(\frac{1 - V_1 V_2}{V_1 - V_2}\right)^2 - 1}, \\ c_1 = \left(\frac{1+\Gamma}{1-\Gamma}\right)^2, \\ c_2 = -\left[\frac{c}{\omega d} \ln\left(\frac{1 - V_1 \Gamma}{V_1 - \Gamma}\right)\right]^2, \end{gathered} \tag{1}$$

from which the electrical and magnetic material parameters follows:

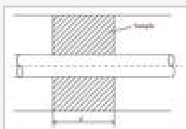

Figure 1: Coaxial line with annular disk of material.

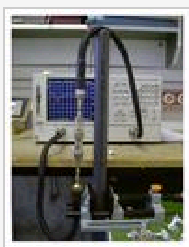

Figure 2: Measurement setup.

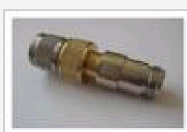

Figure 3: Coaxial line sample holder.

$$\begin{aligned} \mu_R &= \sqrt{c_1 c_2}, \\ \varepsilon_R &= \sqrt{\frac{c_1}{c_2}}. \end{aligned} \tag{2}$$

The sample holder used with the support of teflon beads and the removable connector is shown in Figure 4.

Figure 4: Signal flow graph of sample holder.

Figure 5: Reflection measurements for S^a.

Figure 4 shows the signal flow graph for the measurement system with connectors and the sample holder in the middle. The S^a and S^b represent the reflections and transmissions of the connectors and joints, but not including the sample holder itself which is an air-filled coaxial line in empty stage and has S^o scattering matrix. The resulting S-matrix is S^e.

The S^a and S^b only differ in terms of S_{12} and S_{21}; this leads to the length difference of the two conductors inside the support beads and connectors:

$$S_{11}^a = S_{11}^b, \quad S_{22}^a = S_{22}^b. \tag{3}$$

The sample holder is assumed to be symmetric, reciprocal, lossless, and nonreflecting; therefore,

$$S_{12}^o = S_{21}^o = e^{-jkd}, \quad S_{11}^o = S_{22}^o = 0. \tag{4}$$

The resulting S-matrix S^e and S^a, and S^b is assumed to be reciprocal; therefore,

$$S_{12}^a = S_{21}^a, \quad S_{12}^b = S_{21}^b, \quad S_{12}^e = S_{21}^e. \tag{5}$$

The sample holder has a removable connector only at one side, therefore, directly only S^a can be measured using a short load at various positions in the air-filled sample holder.

There are 4 unknowns in (3)–(5) which can be determined by using 4 measurements, from which there are two reflection measurements for S^a using short load at two different positions and there is the measurement of S^e.

The calibration measurements result in the following four equations:

$$\Gamma_{m1} = S_{11}^a - S_{21}^a \cdot S_{12}^a \frac{1}{1+S_{22}^a}, \quad \Gamma_{m2} = S_{11}^a - S_{21}^a \cdot e^{-j2kl} \cdot S_{12}^a \frac{1}{1+S_{22}^a \cdot e^{-j2kl}}, \tag{6}$$

where Γ_{m1} and Γ_{m2} are the two measured reflection coefficients for S^a using short load at two different positions:

$$S_{11}^e = S_{11}^a + S_{21}^a \cdot e^{-j2kd} \cdot S_{22}^b \frac{1}{1 - S_{22}^a \cdot S_{22}^b \cdot e^{-j2kd}} S_{12}^a, \quad S_{21}^e = S_{21}^a \cdot e^{-jkd} \frac{1}{1 - S_{22}^a \cdot S_{22}^b \cdot e^{-j2kd}} S_{21}^b. \tag{7}$$

The solutions for the four unknowns are

$$\left(S_{22}^a\right)_{1,2} = \frac{-K_1\left(e^{-j2kl} + e^{-j2kd}\right) \pm \sqrt{Q-Z}}{2 \cdot \left(K_2 e^{-j2kd} + K_1 e^{-j2k(l+d)}\right)}, \tag{8}$$

$$S_{12}^a = \sqrt{\frac{\left(S_{11}^e - \Gamma_{m1}\right)\left(1+S_{22}^a\right)\left(1 - e^{-j2kd} \cdot \left(S_{22}^a\right)^2\right)}{1 + S_{22}^a \cdot e^{-j2kd}}}, \tag{9}$$

$$S_{11}^a = \Gamma_{m1} + \frac{\left(S_{12}^a\right)^2}{1+S_{22}^a}, \tag{10}$$

$$S_{12}^{b} = \frac{S_{21}^{e}\left(1 - e^{-j2kd}\left(S_{22}^{a}\right)^{2}\right)}{S_{12}^{a} \cdot e^{-jkd}}, \tag{11}$$

where $Q = K_1^2(e^{-j2kl} + e^{-j2kd})^2$ and $Z = 4(K_1 - K_2)(K_2 e^{-j2kd} + K_1 e^{-j2k(l+d)})$,

$$K_1 = \frac{\Gamma_{m2} - \Gamma_{m1}}{1 - e^{-j2kl}},$$
$$K_2 = S_{11}^{e} - \Gamma_{m1}, \tag{12}$$
$$\left|S_{22}^{a}\right| \leq 1.$$

Figure 6 shows the angle of $S_{12}{}^{a}$ and $S_{12}{}^{b}$ evaluated from (9) and (11) and based on calibration measurements. There is only a slight difference between them which gives proofs to the previous assumptions (3)–(5) but also confirms the small deviation in length and geometry between the two connector parts.

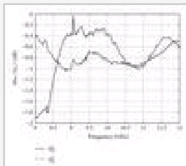

Figure 6: $S_{12}{}^{a}$ and $S_{12}{}^{b}$ used for compensation of measurements.

2.2. Measurement Errors

The main sources of errors are the higher-order modes propagating on the coaxial sample holder, measuring line and the sample size with placement errors.

2.2.1. Higher Mode Propagation

The higher modes can be suppressed using smaller diameter coaxial line. This effect is illustrated in Figure 7 using 7/3 mm coaxial line outer/inner diameters. The relative measurement error for typical high-frequency ferrite material ($\varepsilon = 2 - 0.8j$, $\mu = 5 - 1j$) is below 1.5%. The error reduction or the measurement frequency extension is possible by reducing the measurement line diameter.

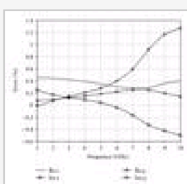

Figure 7: Higher mode propagation effect.

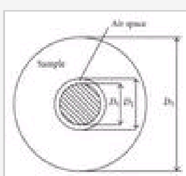

Figure 8: Sample diameters for air gap correction.

The main effect was investigated and analyzed, which is related to the sample size and causes the main errors in measurements.

2.2.2. The Effect of Air Gap between the Sample and the Coaxial Line

The effect of a small air gap caused by manufacturing tolerances was investigated. The measuring error is more significant in case if the air gap is at the inner conductor of the coaxial line so this effect was analyzed.

The effect causes error in permittivity and permeability. The error in permittivity can be corrected with a simple correction routine. The corrected values are

$$\operatorname{Re}\varepsilon_{corr.} = \operatorname{Re}\varepsilon_{meas.} \frac{\ln(D_3/D_2)}{\ln(D_3/D_1) - \operatorname{Re}\varepsilon_{meas.}\ln(D_2/D_1)},$$
$$\operatorname{Im}\varepsilon_{corr.} = \operatorname{Re}\varepsilon_{corr.} \frac{\operatorname{Im}\varepsilon_{meas.}}{\operatorname{Re}\varepsilon_{meas.}}\left(1 + \operatorname{Re}\varepsilon_{corr.} \frac{\ln(D_2/D_1)}{\ln(D_3/D_2)}\right). \quad (13)$$

Similar expressions can be derived for the permeability correction.

For proving the correction equations, simulations were performed using the HFSS 3D simulator and using the arrangement in Figures 9-10.

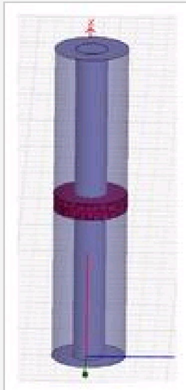

Figure 9: HFSS model of sample holder.

Figure 10: Modeling of sample air gap.

The effect of 0.1 mm air gap on the electrical parameters is shown in Figure 11, where the imperfect sample size is modeled and from the HFSS simulated S_{11} and S_{12} values the ε and μ were calculated using (1)-(2). Then the correction equations (13) are used and the remaining errors are presented in Figure 12.

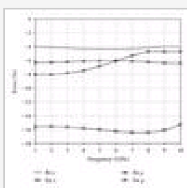

Figure 11: Material parameter measurement error caused by 0.1 mm air gap.

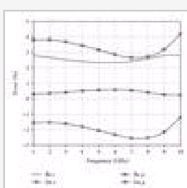

Figure 12: Measurement error corrected.

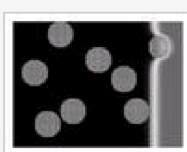

Figure 13: Plane wave propagating between randomly distributed small particles.

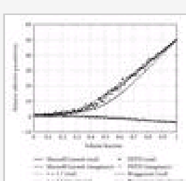

Figure 14: Mixing rules and FDTD simulation results of material mixture.

With the above correction, the measuring error can be decreased to 4% in the frequency range of 1–10 GHz for typical materials for air gap less than 0.1 mm.

3. Microscopic Material Parameters

The material parameters of small sizes of particles in nanomaterials cannot be measured directly by using the conventional measuring methods, thus indirect procedure is suggested. The nanoparticles are solved in known fluid material and in known volume fraction.

Estimating of material parameters of particles in host materials there exist different mixing rules depending on particle interaction effects. The main mixing rules are

Maxwell Garnett mixing rule

$$\varepsilon_{\text{eff}} = \varepsilon_e + 2f\varepsilon_e \frac{\varepsilon_i - \varepsilon_e}{\varepsilon_i + \varepsilon_e - f(\varepsilon_i - \varepsilon_e)}, \tag{14}$$

and Bruggeman mixing rule [2]

$$(1-f)\frac{\varepsilon_e - \varepsilon_{\text{eff}}}{\varepsilon_e + 2\varepsilon_{\text{eff}}} + f\frac{\varepsilon_i - \varepsilon_{\text{eff}}}{\varepsilon_i + 2\varepsilon_{\text{eff}}} = 0, \tag{15}$$

where ε_{eff} is the effective permittivity of the mixture, where spherical inclusions with permittivity ε_i occupy a volume fraction f in a host material ε_e.

The Maxwell Garnett and Bruggeman are the special cases of a general mixing rule

$$\frac{\varepsilon_{\text{eff}} - \varepsilon_e}{\varepsilon_{\text{eff}} + 2\varepsilon_e + v(\varepsilon_{\text{eff}} - \varepsilon_e)} = f\frac{\varepsilon_i - \varepsilon_e}{\varepsilon_i + 2\varepsilon_e + v(\varepsilon_{\text{eff}} - \varepsilon_e)}. \tag{16}$$

The v dimensionless parameter $v = 1$ gives the Maxwell Garnett rule, $v = 2$ gives the Bruggeman formula, and $v = 3$ gives the coherent potential approximation.

A similar mixing formula (Bruggeman) can be obtained for the permeability

$$f\frac{\mu_i - \mu_{\text{eff}}}{\mu_i + \mu_{\text{eff}}} + (1-f)\frac{\mu_e - \mu_{\text{eff}}}{\mu_e + \mu_{\text{eff}}} = 0, \tag{17}$$

where μ_{eff} is the effective permeability of the mixture, and spherical inclusions with permeability μ_i occupy a volume fraction f in a host material μ_e.

Two-dimensional simulation using an FDTD solver is applied to prove and illustrate the indirect nanoparticle material parameter determination method. Small particles are randomly distributed in two-dimensional areas and an incident wave is propagating on this area, influenced by them. From simulated macroscopic material parameters (16), (17) are verified and the v is determined for practical application [3, 4].

The FDTD simulation results show an effective permittivity, which is close to Bruggeman's approximation but using an error minimization v = 1.7 gives an optimum curve (for $\varepsilon_i = 50 - j^*4.0$, $\varepsilon_e = 2.0 - j^*0$).

4. Conclusion

The main steps of characterization and measurement of microwave absorbent materials in the 1–10 GHz range are introduced for macroscopic and microscopic material parameter determination. The coaxial reflection-transmission type of material parameter measurement is analyzed in detail and measurement error is corrected. Genetic algorithm concept of optimization multilayer antireflection coating is summarized. Two-dimensional FDTD simulations were presented to model the behavior of mixed electric and magnetic type of material.

Acknowledgments

This work was supported by the ACE2 European FP6 framework program and OMFB-00252/2007 Project.

References

1. L. Nagy, "An improved TDR method for determining material parameters," in *Proceedings of the 13th General Assembly of the International Union of Radio Science (URSI '90)*, Prague, Czechoslovakia, August 1990.
2. D. A. G. Bruggeman, "Berechnung verschiedener physikalischer Konstanten von heterogenen Substanzen. I. Dielektrizitätskonstanten und Leitfähigkeiten der Mischkörper aus isotropen Substanzen," *Annalen der Physik*, vol. 416, no. 7, pp. 636–664, 1935.
3. K. K. Kärkkäinen, A. H. Sihvola, and K. I. Nikoskinen, "Analysis of a three-dimensional dielectric mixture with finite difference method," *IEEE Transactions on Geoscience and Remote Sensing*, vol. 39, no. 5, pp. 1013–1018, 2001.
4. K. K. Kärkkäinen, A. H. Sihvola, and K. I. Nikoskinen, "Effective permittivity of mixtures: numerical validation by the FDTD method," *IEEE Transactions on Geoscience and Remote Sensing*, vol. 38, no. 3, pp. 1303–1308, 2000.